ASTROPHYSICS

Asymmetry study of the mixed-morphology supernova remnant G 18.95-1.1

A.M. Bykov[1], Yu.A. Uvarov[1] ✉

[1] Ioffe Institute, St. Petersburg, Russia

✉ uv@astro.ioffe.ru

Abstract. Radio and X-ray maps of supernova remnants (SNRs) in many cases revealed an asymmetric global structure. This may reflect the inhomogeneity of the circumstellar/ambient matter, anisotropic energy release or both. Given a growing sample of the observed SNRs some techniques to characterize the global asymmetry are needed to identify old SNRs in sky surveys among other observed extended structures of low surface brightness. We discuss here the applications of modified power-ratio technique to quantify the global asymmetry of the mixed-morphology SNR G 18.95-1.1 using its recent mapping with SRG and compare results with the well-studied SNRs IC 443 and Cas A.

Keywords: supernova remnants, SNR, power-ratio method

Исследование асимметрии остатка сверхновой смешанной морфологии G 18.95-1.1

А.М. Быков[1], Ю.А. Уваров[1] ✉

[1] Физико-технический институт им. А.Ф. Иоффе РАН, Санкт-Петербург, Россия

✉ uv@astro.ioffe.ru

Аннотация. Радио и рентгеновские наблюдения остатков сверхновых (ОСН) во многих случаях выявили их асимметричную глобальную структуру. Эта асимметрия может отражать неоднородность окружающего вещества, анизотропное выделение энергии взрыва или и то, и другое. Учитывая растущее число обнаруженных ОСН, необходимы методы для измерения и классификации их наблюдаемой асимметрии, в том числе для идентификации старых ОСН в обзорах неба среди других наблюдаемых протяженных структур с низкой поверхностной яркостью. Мы обсуждаем применение модифицированного метода отношений моментов для количественной оценки глобальной асимметрии ОСН смешанного типа G 18.95-1.1, на основе его недавних наблюдений обсерваторией СРГ, и сравниваем полученные результаты с результатами анализа хорошо изученных ОСН IC 443 и Cas A.

Ключевые слова: остатки сверхновых, ОСН, метод отношения моментов

Introduction

Mixed-morphology SNRs comprise a subclass of more than 40 SNRs with shell-type radio images and a central-filled thermal X-ray maps (see [1−3] for a review). A mixed-morphology supernova remnant G 18.95-1.1 was studied in a broad energy range from radio to X-rays. It was discovered by Fuerst et al. [4] in the radio survey of the galactic plane [5]. In H_α it was studied in [6]. X-ray observations with ROSAT [7, 8], ASCA [9], Chandra [10] and recently SRG [11] established a highly anisotropic shape with a bunch of bright emission clumps in the south with a prominent line emission, dim north part and a likely pulsar wind nebula (PWN) in the center elongated to the north. Bright southern clumps line emission shows an excess of element abundances over the solar values which is typical for ejecta fragments [11]. These features can be understood if G18.95-1.1 is a result of the asymmetric supernova explosion with a progenitor star interior material ejected to the south and a pulsar kick directed to the north. An asymmetric mass ejection right after the supernova core collapse was modelled, e.g., in [12] while the subsequent sphericization of the remnants in the isotropic interstellar medium was discussed earlier in [13]. To quantify the global asymmetric morphology of SNRs in [14] was proposed the power-ratio technique which modified version we apply here to the recent detailed maps of SNR G18.95-1.1 [11] obtained with SRG X-ray observatory [15]. A similar analyses of the asymmetry of IC443 and Cas A SNRs are also discussed for a comparison.

IC 443 (G189.1+3.0) is an extended and old SNR (~ 45′ size at a distance of 1.5 kpc [16]). In radio bands it shows two half shell structure [17]. This is considered to be an effect of an interaction with a torus-like molecular cloud [18, 19] that separates two half-shells. In X-rays it was studied with ROSAT [20], ASCA [21, 22], BeppoSAX [23], Chandra [24−26], XMMNewton [27, 28, 19], and RXTE [29]. XMM-Newton mosaic exposure corrected X-ray image in the 0.4−8.0 keV energy range is shown in Fig. 1. X-ray emission morphology is center-filled with maximum emission in the north and a bright clump of the emission in the south (1SAX J0618.0+2227). This southern source is considered to be a PWN [24, 25, 27]. There is a bunch of clump-like sources in the southern part that could be considered as interaction cites of the ejecta fragments and a molecular cloud [28, 30].

Cas A is a young and bright SNR that was studied in depth in all of the spectral bands: radio [31−33], optical [34], infrared [35, 36], X-rays [37, 38]. The total Chandra exposure used for observation of this remnant exceeds 1 Ms that allows construction of high resolution X-ray image of the SNR (Fig. 1) that shows a remarkable source structure.

To analyze morphology of the discussed above SNRs shown in Fig. 1 we apply a modified power-ratio technique. This technique was developed in [39, 40] for studies of galactic clusters.

Then it was successfully applied to study asymmetric structure of a set of SNRs in [14, 41−44]. The method is described in the next section.

Methods

The power-ratio method is based on the multipole expansion of the 2D gravitation potential within the circular aperture with radius R:

$$\Psi(R,\phi) = -a_0 ln(1/R) - \sum_{m=1}^{\infty} \left(a_m cos(m\phi) + b_m sin(m\phi)\right) / mR^m,$$

$$a_m = \int_{r'<R} \Sigma(r',\phi) cos(m\phi) r'^{m+1} dr' d\phi,$$

$$b_m = \int_{r'<R} \Sigma(r',\phi) sin(m\phi) r'^{m+1} dr' d\phi,$$

Here $\Sigma(r,\phi)$ is the surface mass density inside the aperture. In practice the surface mass density is not known and a X-ray brightness distribution is used instead. Thus $\Sigma(r,\phi)$ is not directly connected with the surface mass density and actually this method is no more than the multipole expansion for the surface brightness filtered by aperture that allows one to make a classification of the structure of studied objects. The power of the multipole expansion is calculated as:

$$P(R) = \frac{1}{2\pi} \int_0^{2\pi} \Psi_m(R,\phi)\,\Psi_m(R,\phi)\,d\phi,$$

$$P_0 = \left(a_0 ln(R)\right)^2, \quad P_m = \frac{a_m^2 + b_m^2}{2m^2 R^{2m}}.$$

(1)

Usually the dimensionless ratio P_m/P_0 is measured and the origin of coordinate system is chosen in the center of brightness so $P_1 = 0$. However, $P_m/P_0 \sim 1/R^{2m} ln^2(R)$ is aperture size dependent value that makes a comparison of these ratios for objects with different sizes not straightforward. We suggest instead calculating amplitudes $\tilde{a}_m, \tilde{b}_m$ of multipole expansion in the dimensionless coordinates r/R_* where R_* is a characteristic radius of the studied object. We define R_* to be the radius of the minimum circle aperture fully enclosing the object. In this case, $a_m = R_*^{m+2} \tilde{a}_m, b_m = R_*^{m+2} \tilde{b}_m$. We also suggest using ratios $\tilde{P}_m / \tilde{a}_0^2$ for the analyses which are dimensionless, don't depend on object size and reflects the object structure. We use these notations below for study G18.95-1.1, IC 443 and Cas A SNRs.

However, usually SNR outer borders are not sharp enough and some diffuse background emission is present that allows a systematic error in the definition of R_*. It also should be mentioned that the integrand expressions for a_m, b_m are growing as r^{m+1} with r and thats why even small background emission far outside the source can dramatically spoil the moment estimations if it is included in the integration. So clearing the emission map from background point sources and diffuse emission is essential. This is made in tree steps. At first point sources are filtered out. Then the diffuse background emission outside the R_* aperture is estimated and subtracted from the image. At last the emission outside the aperture is set to zero. After this the values $\tilde{P}_m / \tilde{a}_0^2$ are independent from the aperture size $R > R_*$ enclosing the circle R_* if the value R_* is used for R in the Eq. (1). However, these values are dependent on the position of the origin of coordinate system. In particular, $\tilde{P}_1 = 0$ if and only if the origin coincides with the center of brightness.

The systematic errors arising from the uncertainty of R_* can be estimated by comparison of the results obtained for different values of R_*. The stochastic errors arising because of the Poisson nature of the incoming photons can be calculated with the Monte-Carlo simulation of a set of X-ray images as was done in [41].

Results

We demonstrate the application of the power-ratio method for study G18.95-1.1, IC 443 and Cas A SNRs. Cas A has an almost spherically symmetric shell. However there is a special structure in the north-east part of the shell that is considered to be a trace of the jet formed during SN explosion. IC 443 is a well-known example of the SNR interacting with a molecular cloud. G18.95-1.1 is considered to be an example of an asymmetric SN explosion [11].

Fig. 1 shows X-ray maps of the studied SNRs and demonstrates the analyses used. G18.95-1.1 map was constructed as a result of SRG/eROSITA observations (panel (*a*), [11]). Panel (*b*) shows the same map with point sources filtered out including pulsar candidate (P) and bright source (1) associated with a star [11]. IC 443 map is constructed as a mosaic image of XMM-Newton observations using ESAS[1] software (panel (*c*)). Panel (*d*) shows the same map with point sources filtered out together with PWN candidate that with some probability belongs to an other SNR G189.6+3.3 [24−27] overlapping with IC 443. Cas A X-ray image was obtained using Chandra data. The center point source was filtered out in the analyses. O and X points show the geometrical center of the apertures and the center of brightness. Apertures R_* that were used for estimation of the systematic errors of momentum estimations are also shown for all studied remnants.

_____

[1] http://www.cosmos.esa.int/web/xmm-newton/xmm-esas
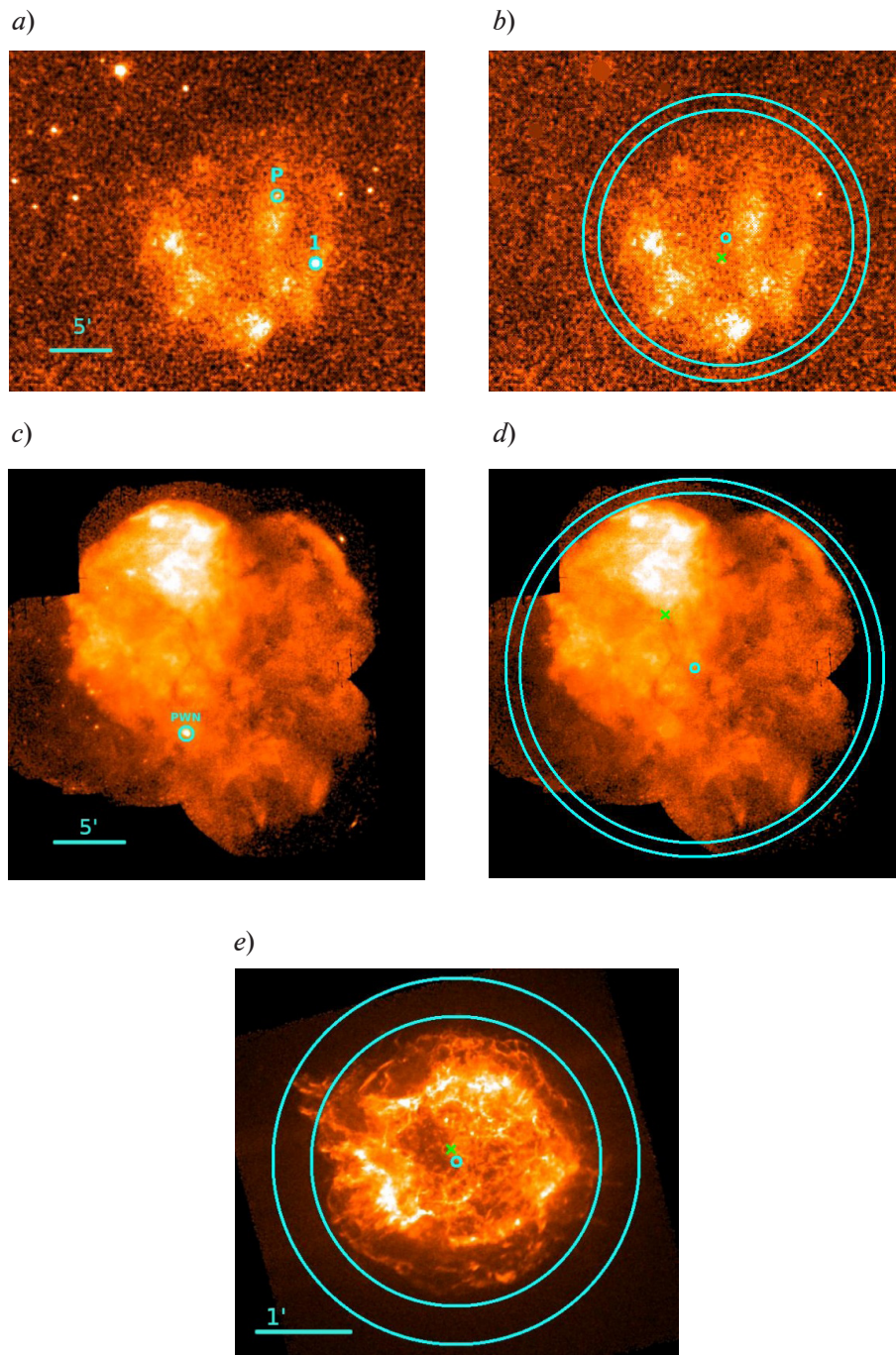
Fig. 1. X-ray maps of studied SNRs. Upper panels show SRG/eROSITA map (0.5−2.3 keV) of the G18.95-1.1 with (*a*) and without (*b*) filtering of point sources. Middle panels show XMMNewton map (0.4−8.0 keV) of the IC443 produced with ESAS software with (*c*) and without (*d*) filtering of point sources and PWN region. Lower panel (*e*) shows Chandra map (0.4−8.0 keV) of the Cas A. Different apertures R_* used for systematic errors estimations are shown as cyan circles whose radius values are listed in Tables 1,2. O and X points show the geometrical center of the apertures and the center of brightness

Tables 1, 2 list calculated values $\tilde{P}_m / \tilde{a}_0^2$ for $m = 1, 2, 3, 4$ for each values of R_* used. Table 1 lists the results for the case when the origin of coordinate system coincides with the center of brightness so $\tilde{P}_1 = 0$. Table 2 lists the results for the case when the origin coincides with the center of aperture. 1σ statistical error due to Poisson statistic of the incoming photons, listed in the Tables, was calculated in Monte-Carlo simulations of the emission maps with 1000 iterations and subsequent image smoothing with the same criteria that was used to construct an initial map.

Table 1

Values of $\tilde{P}_m / \tilde{a}_0^2$ for $m = 2, 3, 4$
Center of brightness coordinate system

object	R_*, arcmin	$\tilde{P}_2 / \tilde{a}_0^2$	$\tilde{P}_3 / \tilde{a}_0^2$	$\tilde{P}_4 / \tilde{a}_0^2$
G 18.95-09	21.6	$(8.0\pm0.4)\cdot10^{-5}$	$(3.9\pm0.2)\cdot10^{-5}$	$(4.2\pm0.3)\cdot10^{-6}$
	19.2	$(5.6\pm0.3)\cdot10^{-5}$	$(3.3\pm0.1)\cdot10^{-5}$	$(2.8\pm0.2)\cdot10^{-6}$
IC 443	27.0	$(9.50\pm0.05)\cdot10^{-4}$	$(4.75\pm0.05)\cdot10^{-5}$	$(1.85\pm0.01)\cdot10^{-4}$
	25.0	$(9.20\pm0.05)\cdot10^{-4}$	$(4.85\pm0.05)\cdot10^{-5}$	$(1.75\pm0.01)\cdot10^{-4}$
Cas A	3.9	$(4.03\pm0.04)\cdot10^{-4}$	$(2.70\pm0.03)\cdot10^{-5}$	$(2.60\pm0.03)\cdot10^{-6}$
	3.1	$(3.60\pm0.01)\cdot10^{-4}$	$(3.42\pm0.01)\cdot10^{-5}$	$(1.14\pm0.01)\cdot10^{-6}$

N o t e : 1σ statistical error due to Poisson photon distribution is listed in the Table.

Table 2

Values of $\tilde{P}_m / \tilde{a}_0^2$ for $m = 1, 2, 3, 4$
Center of aperture coordinate system

object	R_*	$\tilde{P}_1 / \tilde{a}_0^2$	$\tilde{P}_2 / \tilde{a}_0^2$	$\tilde{P}_3 / \tilde{a}_0^2$	$\tilde{P}_4 / \tilde{a}_0^2$
	arcmin	$\times10^{-3}$	$\times10^{-3}$	$\times10^{-3}$	$\times10^{-6}$
G 18.95-09	21.6	10.2 ± 0.1	$(9.8\pm0.4)\cdot10^{-2}$	$(1.5\pm0.1)\cdot10^{-2}$	1.7 ± 0.2
	19.2	9.8 ± 0.1	$(7.7\pm0.3)\cdot10^{-2}$	$(1.4\pm0.1)\cdot10^{-2}$	1.0 ± 0.1
IC 443	27.0	91.9 ± 0.1	9.11 ± 0.01	1.44 ± 0.01	730 ± 1
	25.0	93.2 ± 0.1	9.20 ± 0.01	1.45 ± 0.01	700 ± 1
Cas A	3.9	3.45 ± 0.01	$(3.10\pm0.01)\cdot10^{-1}$	$(2.36\pm0.01)\cdot10^{-2}$	5.42 ± 0.04
	3.1	3.28 ± 0.01	$(2.77\pm0.01)\cdot10^{-1}$	$(2.97\pm0.01)\cdot10^{-2}$	3.57 ± 0.02

Note: 1σ statistical error due to Poisson photon distribution is listed in the Table. Multiplication factors listed in the first row should be applied to the table values of the corresponding columns.

Discussion and Conclusions

In this work three anisotropic SNRs were considered: G18.95-1.1, IC 443 and Cas A. Cas A image has a possible trace of the jet formed during SN explosion, IC 443 is an example of SNR interacting with a molecular cloud and G18.95-1.1 is considered to be a result of an asymmetric SN explosion. We modified the power-ratio method for analyses of the objects with different sizes and applied it for listed SNRs using two different coordinate systems. One of which coincides with the center of brightness and the other with the geometrical center of the object. A center of minimal circular aperture fully enclosing the object was chosen as the geometrical center of SNR.

For both systems of coordinates asymmetry of IC443, which is interacting with a molecular cloud, is characterized by greater values of all 4 moments $\tilde{P}_1, \tilde{P}_2, \tilde{P}_3, \tilde{P}_4$. While G18.95-1.1, that was born in an asymmetric explosion, has higher value of $\tilde{P}_1$ and lower values of $\tilde{P}_2$ and $\tilde{P}_4$, than Cas A, which has more symmetric shell with a trace of a jet. We demonstrate that a modified power-ratio method can be used for the comparative analysis of SNR anisotropy even if angular sizes of studied remnants differ.

REFERENCES

1. **Rho J., Petre R.,** Mixed-Morphology Supernova Remnants, Astrophysical Journal Letters. 503 (1998) L167–L170.

2. **Slane P., et al.,** Supernova Remnants Interacting with Molecular Clouds: X-Ray and Gamma-Ray Signatures, Space Science Reviews. 188 (2015) 187−210.

3. **Vink J.,** Physics and Evolution of Supernova Remnant. Springer, 2020.

4. **Fuerst E., et al.,** A new non-thermal galactic radio source with a possible binary system. Nature, 314 (1985) 720−721.

5. **Reich W., et al.,** A radio continuum survey of the galactic plane at 11cm wavelenght. I. The area 357.4 < or = L < or = 76, - 1.5 < or = B < or = 1.5, Astronomy and Astrophysics Supplement Series. 58 (1984) 197−248.

6. **Stupar M., Parker Q.A.,** Catalogue of known Galactic SNRs uncovered in Halpha light, Monthly Notices of the RAS. 414 (2011) 2282−2296.

7. **Aschenbach B., et al.,** Observation of soft X-ray emission from the supernova remnant G 18.95-1.1, Astronomy and Astrophysics. 246 (1991) L32−L35.

8. **Fuerst E., Reich W., Aschenbach B.,** New radio and soft X-ray observations of the supernova remnant G 18.95-1.1, Astronomy and Astrophysics. 319 (1997) 655−663.

9. **Harrus I.M., et al.,** An X-Ray Study of the Supernova Remnant G18.95-1.1, Astrophysical Journal. 603 (2004) 152−158.

10. **Tüllmann R., et al.,** Searching for the Pulsar in G18.95-1.1: Discovery of an X-ray Point Source and Associated Synchrotron Nebula with Chandra, Astrophysical Journal. 720 (2010) 848−852.

11. **Bykov A.M., et al.,** Spatially resolved X-ray spectra of the Galactic SNR G18.95-1.1: SRG/eROSITA view, Astronomy and Astrophysics. 661 (2022) A19–28.

12. **Janka H.T.,** Neutron Star Kicks by the Gravitational Tug-boat Mechanism in Asymmetric Supernova Explosions: Progenitor and Explosion Dependence, Astrophysical Journal. 837 (2017) 84.

13. **Bisnovatyj-Kogan G.S., Blinnikov S.I.,** Sphericization of the Remnants of an Asymmetric Supernova Outburst in a Homogeneous Medium, Soviet Astronomy. 26 (1982) 530−537.

14. **Holland-Ashford T., et al.,** Comparing Neutron Star Kicks to Supernova Remnant Asymmetries, Astrophysical Journal. 844 (2017) 84–99.

15. **Sunyaev R., et al,** SRG X-ray orbital observatory. Its telescopes and first scientific results, Astronomy and Astrophysics. 656 (2021) A132.

16. **Fesen R.A., Kirshner R.P.,** Spectrophotometry of the supernova remnant IC 443, Astrophysical Journal. 242 (1980) 1023−1040.

17. **Green D.A.,** Constraints on the secular decrease in the flux density of CAS A at 13.5, 15.5 and 16.5 GHz, Monthly Notices of the RAS. 221 (1986) 473−482.

18. **Burton M.G., et al,** Shocked molecular hydrogen in the supernova remnant IC 443, Monthly Notices of the RAS. 231 (1988) 617−634.

19. **Troja E., Bocchino F., Reale F.,** XMM-Newton Observations of the Supernova Remnant IC 443. I. Soft X-Ray Emission from Shocked Interstellar Medium, Astrophysical Journal. 649 (2006) 258−267.

20. **Asaoka I., Aschenbach B.,** An X-ray study of IC443 and the discovery of a new supernova remnant by ROSAT, Astronomy and Astrophysics. 284 (1994) 573−582.

21. **Keohane J.W., et al.,** A Possible Site of Cosmic Ray Acceleration in the Supernova Remnant IC 443, Astrophysical Journal. 484 (1997) 350−359.

22. **Kawasaki M.T., et al.,** ASCA Observations of the Supernova Remnant IC 443: Thermal Structure and Detection of Overionized Plasma, Astrophysical Journal. 572 (2002) 897−905.

23. **Bocchino F., Bykov A.M.,** Hard X-ray emission from IC443: evidence for a shocked molecular clump?, Astronomy and Astrophysics. 362 (2000) L29−L32.

24. **Olbert C.M., et al.,** A Bow Shock Nebula around a Compact X-Ray Source in the Supernova Remnant IC 443, Astrophysical Journal. 554 (2001) L205−L208.

25. **Gaensler B.M., et al.,** The X-Ray Structure of the Pulsar Bow Shock G189.22+2.90 in the Supernova Remnant IC 443, Astrophysical Journal. 648 (2006) 1037−1042.

26. **Weisskopf M.C., et al.,** Chandra observations of neutron stars: an overview, Astrophysics and Space Science. 308 (2007) 151−160.

27. **Bocchino F., Bykov A.M.,** The plerion nebula in IC 443: The XMM-Newton view, Astronomy and Astrophysics. 376 (2001) 248−253.

28. **Bocchino F., Bykov A.M.,** XMM-Newton study of hard X-ray sources in IC 443, Astronomy and Astrophysics. 400 (2003) 203−211.

29. **Sturner S.J., Keohane J.W., Reimer O.,** Observation of non-thermal emission from the supernova remnant IC 443 with RXTE, Advances in Space Research. 33 (2004) 429−433.

30. **Bykov A.M., et al.,** Isolated X-Ray-Infrared Sources in the Region of Interaction of the Supernova Remnant IC 443 with a Molecular Cloud, Astrophysical Journal. 676 (2008) 1050−1063.

31. **Anderson M.C., Rudnick L.,** Sites of Relativistic Particle Acceleration in Supernova Remnant Cassiopeia A, Astrophysical Journal. 456 (1996) 234.

32. **Kassim N.E., et al.,** Evidence for Thermal Absorption inside Cassiopeia A, Astrophysical Journal. 455 (1995) L59.

33. **O'Sullivan C., Green D.A.,** Constraints on the secular decrease in the flux density of CAS A at 13.5, 15.5 and 16.5 GHz, Monthly Notices of the RAS. 303 (1999) 575−578.

34. **Fesen R.A., et al.,** Ejecta Knot Flickering, Mass Ablation, and Fragmentation in Cassiopeia A, Astrophysical Journal. 736 (2011) 109.

35. **Koo B.C., et al.,** A Deep Near-infrared [Fe II] + [Si I] Emission Line Image of the Supernova Remnant Cassiopeia A, Astrophysical Journal. 866 (2018)139.

36. **Vogt F.P.A., et al.,** Probing Interstellar Dust with Infrared Echoes from the Cas A Supernova, Astrophysical Journal. 750 (2012) 155.

37. **Gotthelf E.V., et al.,** Chandra Detection of the Forward and Reverse Shocks in Cassiopeia A, Astrophysical Journal. 552 (2001) L39−L43.

38. **Sato T., et al.,** X-Ray Measurements of the Particle Acceleration Properties at Inward Shocks in Cassiopeia A, Astrophysical Journal. 853 (2018) 46.

39. **Buote D.A., Tsai J.C.,** Quantifying the Morphologies and Dynamical Evolution of Galaxy Clusters. I. The Method, Astrophysical Journal. 452 (1995) 522.

40. **Buote D.A., Tsai J.C.,** Quantifying the Morphologies and Dynamical Evolution of Galaxy Clusters. II. Application to a Sample of ROSAT Clusters, Astrophysical Journal. 458 (1996) 27.

41. **Lopez L.A., et al.,** Typing Supernova Remnants Using X-Ray Line Emission Morphologies, Astrophysical Journal. 706 (2009) L106−L109.

42. **Lopez L.A., Fesen R.A.,** The Morphologies and Kinematics of Supernova Remnants, Space Science Reviews. 214 (2018) 44.

43. **Holland-Ashford T., Lopez L.A., Auchettl K.,** Asymmetries of Heavy Elements in the Young Supernova Remnant Cassiopeia A, Astrophysical Journal. 889 (2020) 144–152.

44. **Picquenot A., et al.,** Three-dimensional morphological asymmetries in the ejecta of Cassiopeia A using a component separation method in X-rays, Astronomy and Astrophysics. 646 (2021) A82–A94.

THE AUTHORS

UVAROV Yury A.
uvy@mail.ru
ORCID: 0000-0002-4962-5437

BYKOV Andrei M.
byk@astro.ioffe.ru
ORCID: 0000-0003-0037-2288